Enhanced Self-Assembly and Mechanical Properties of Cellulose-Based Triblock Copolymers: Comparisons with Amylose-Based Triblock Copolymers

Satoshi Katsuhara,[a] Yasuko Takagi,[a] Naoki Sunagawa,[b] Kiyohiko Igarashi,[b, c] Takuya Yamamoto,[d] Kenji Tajima,[, d] Takuya Isono,*[, d] Toshifumi Satoh*[, d]*

[a]Graduate School of Chemical Sciences and Engineering, Hokkaido University, Sapporo 060-8628, Japan.

[b]Department of Biomaterial Sciences, Graduate School of Agriculture and Life Sciences, The University of Tokyo, Tokyo 113-8657, Japan.

[c]VTT Technical Research Centre of Finland Ltd., VTT FI-02044, Finland; Department of Biomaterial Sciences, Graduate School of Agriculture and Life Sciences, The University of Tokyo, Tokyo 113-8657, Japan.

[d]Faculty of Agriculture, Niigata University, Niigata 950-2181, Japan.

[e]Faculty of Engineering, Hokkaido University, Sapporo 060-8628, Japan.

AUTHOR INFORMATION

Corresponding Authors

Kenji Tajima – *Faculty of Engineering, Hokkaido University, Sapporo 060-8628, Japan*; ORCID 0000-0002-3238-813X; Email: ktajima@eng.hokudai.ac.jp

Takuya Isono – *Faculty of Engineering, Hokkaido University, Sapporo 060-8628, Japan*; ORCID 0000-0003-3746-2084; Email: isono.t@eng.hokudai.ac.jp

Toshifumi Satoh – *Faculty of Engineering, Hokkaido University, Sapporo 060-8628, Japan*; ORCID 0000-0001-5449-9642; Email: satoh@eng.hokudai.ac.jp

Authors

Satoshi Katsuhara – *Graduate School of Chemical Sciences and Engineering, Hokkaido University, Sapporo 060-8628, Japan*; Email: satoshi-k@eis.hokudai.ac.jp

Yasuko Takagi – *Graduate School of Chemical Sciences and Engineering, Hokkaido University, Sapporo 060-8628, Japan*; Email: y.takagi.0319@gmail.com

Naoki Sunagawa – *Department of Biomaterial Sciences, Graduate School of Agriculture and Life Sciences, The University of Tokyo, Tokyo 113-8657, Japan*; ORCID 0000-0002-0382-6671; Email: sunagawa.naoki@mail.u-tokyo.ac.jp

Kiyohiko Igarashi – *VTT Technical Research Centre of Finland Ltd., VTT FI-02044, Finland; Department of Biomaterial Sciences, Graduate School of Agriculture and Life Sciences, The University of Tokyo, Tokyo 113-8657, Japan*; ORCID 0000-0001-5152-7177; Email: KIYOIGRS@kb3.so-net.ne.jp

Takuya Yamamoto – *Faculty of Engineering, Hokkaido University, Sapporo 060-8628, Japan*; ORCID 0000-0001-9716-8237; Email: yamamoto.t@eng.hokudai.ac.jp

KEYWORDS: Self-assembly, block copolymers, amylose, cellulose, sustainable elastomers.

ABSTRACT

Herein, we compared the microphase-separation behavior and mechanical properties of cellulose- and amylose-based block copolymers (BCPs). Various cellooligosaccharide triacetate-*b*-poly(*δ*-decanolactone)-*b*-cellooligosaccharide triacetates (AcCel$_n$-*b*-PDL-*b*-AcCel$_n$s), which are cellulose-based ABA-type BCPs, with PDL molecular weights of approximately 5, 10, and 20 kg mol^{-1} and PDL volume fractions of 0.65, 0.77, and 0.87, were synthesized from *α*,*ω*-diazido-end-functionalized PDLs and propargyl-end-functionalized cellooligosaccharide triacetates via click chemistry. We adopted the cellodextrin-phosphorylase-mediated oligomerization of *α*-D-glucose-1-phosphase in the presence of a propargyl-end-functionalized cellobiose primer to synthesize the functional cellooligosaccharide segment. The maltooligosaccharide triacetate-*b*-poly(*δ*-decanolactone)-*b*-maltooligosaccharide triacetate (AcMal$_n$-*b*-PDL-*b*-AcMal$_n$s) amylose counterparts were also synthesized in a similar manner. Small-angle X-ray scattering experiments and atomic force microscopy revealed that the AcCel$_n$-*b*-PDL-*b*-AcCel$_n$s are more likely to microphase-separate into ordered nanostructures compared to the AcMal$_n$-*b*-PDL-*b*-AcMal$_n$s, despite their comparable chemical compositions and molecular weights. Furthermore, the AcCel$_n$-*b*-PDL-*b*-AcCel$_n$s exhibited significantly superior mechanical performance compared to their amylose counterparts under tensile testing, with the Young's modulus and stress at break of AcCel$_n$-*b*-PDL$_{10k}$-*b*-AcCel$_n$ being 2.3- and 1.8-times higher, respectively, than those of AcMal$_n$-*b*-PDL$_{10k}$-*b*-AcMal$_n$. The enhanced microphase-separation and mechanical properties of the AcCel$_n$-*b*-PDL-*b*-AcCel$_n$s were found to be attributable to the stiffness and crystalline nature of the AcCel$_n$ segments. These results demonstrate the advantages of using cellulose derivatives to synthesize novel bio-functional materials.

Introduction

The development of polymeric materials from natural and renewable resources has recently gained international momentum in order to mitigate the increasing environmental issues.[1–3] Carbohydrates are particularly interesting as renewable raw materials because they are readily available from a wide range of plant biomass resources, such as sugar corn, sugarcane, seaweed, waste wood, and agricultural waste.[1] Furthermore, the unique characteristics of carbohydrates, including their biocompatibilities, biodegradabilities, strong hydrophilicities, optical activities, and low toxicities, make them significantly attractive raw materials for creating novel sustainable polymers. Currently, the polymer industry employs carbohydrates mostly as carbon resources for producing bioplastics, such as polylactide, poly(3-hydroxybutyric acid), poly(ethylene furanoate), and poly(2,5-furandicarboxylic acid), through chemical or fermentation processes, despite the fact that cellulose and its derivatives have been used as precursors in their native states.[1–3] Using carbohydrates in their native or marginally modified forms may save the energy and time required to transform them to green and sustainable materials, while preserving their unique characteristics.

Directly combining carbohydrate molecules with synthetic polymers is an effective method for achieving the abovementioned goals; this combination can be achieved mainly through grafting synthetic polymer chains onto polysaccharide main chains,[4–7] grafting poly/oligosaccharide chains onto synthetic polymer main chains,[8,9] and tethering poly/oligosaccharides to synthetic polymers to form block copolymers (BCPs).[10–13] Among these, the approach that creates carbohydrate-based BCPs is particularly attractive because of the microphase-separation and micelle-forming abilities of these polymers, which are useful when designing elastomers,[14–16] lithographic materials,[17–19] electrical materials,[20–23] and drug-delivery nanocarriers.[24–26] Carbohydrate-based BCPs remain neglected compared to the other two carbohydrate-containing polymer types because of the

difficulties associated with their syntheses. Recent progress in polymer chemistry has witnessed the evolution of strategies for the production of carbohydrate-based BCPs since the pioneering syntheses of carbohydrate-based BCPs were published in 1961.[13,27] For example, cellulose-*b*-polystyrene, dextran-*b*-polystyrene, and maltoheptaose-*b*-poly(ε-caprolactone) have been successfully synthesized by radical polymerization and ring-opening polymerization from the reducing end of the carbohydrate segment.[13,28–31] However, such a synthetic strategy is incompatible with ionic polymerization methods. An alternative pathway for producing carbohydrate-BCPs involves the end-to-end coupling of end-functionalized carbohydrates and synthetic polymer segments, to which various synthetic polymer segments can be joined.[11,12,17–19,26] In particular, the copper-catalyzed azido-alkyne cycloaddition (CuAAC) reaction has been widely employed for end-to-end coupling because of its high efficiency, simplicity, and functional group tolerance.[32–34]

Most carbohydrate-based BCPs comprise dextran and amylose. Surprisingly, there are a few reports on cellulose-containing BCPs, although cellulose and amylose comprise glucose and similar primary structures, with the only structural difference being the presence of *α*-1,4 linkages in amylose and *β*-1,4 linkages in cellulose. Consequently, little is known about the self-assembly behavior of cellulose-based BCPs in their solid and solution states, and their fundamental physical properties have not been studied in detail to date. Because cellulose is inedible and is the most abundant polymer on Earth, it is highly attractive as a block partner for constructing carbohydrate-based BCPs. Moreover, it is probable that such cellulose-based BCPs will exhibit enhanced self-assembly properties as well as good mechanical performance because cellulose is highly rigid and crystalline.

However, directly using native cellulose to construct BCPs is significantly challenging because cellulose does not dissolve in common solvents or melt even at high temperatures because of strong inter- and intramolecular hydrogen bonding. This fundamental drawback has historically been overcome by chemically modifying the hydroxyl groups with other functional groups, such as cellulose ethers or esters. Cellulose acetate, one of the most common cellulose derivatives, is readily soluble in common organic solvents and melt-processable. Hence, it has been widely commercialized at different degrees of substitution for use as membranes, textiles, protecting films for polarizers, and cigarette filters. In addition, cellulose acetate has recently gained considerable attention because of its potential biodegradability.[35,36] Therefore, carbohydrate-based BCPs containing cellulose acetate segments are of significant interest in terms of their synthesis, self-assembly, and physical properties. Recently, the groups of Matson, Edgar, and Kamitakahara reported BCPs containing cellulose derivatives such as cellulose acetate-*b*-polybutadiene-*b*-cellulose acetate,[37] cellulose acetate-*b*-oligoamide,[38] and trimethyl cellulose-*b*-poly(ethylene glycol).[39] However, the microphase-separation behavior and mechanical properties of these BCPs have not been investigated. Furthermore, the advantages of using cellulose derivatives over other carbohydrates remain unclear.

Herein, we report a pioneering comparative study of cellulose-based BCPs and their amylose-based counterparts with the aim of unveiling the unique characteristics imparted by cellulose segments. To this end, we designed and synthesized ABA-type cellooligosaccharide- and malooligosaccharide-based BCPs, namely, cellooligosaccharide triacetate-*b*-poly(*δ*-decanolactone)-*b*-cellooligosaccharide triacetates (AcCel$_n$-*b*-PDL-*b*-AcCel$_n$s) and maltooligosaccharide triacetate-*b*-poly(*δ*-decanolactone)-*b*-maltooligosaccharide triacetates (AcMal$_n$-*b*-PDL-*b*-AcMal$_n$s), as shown in **Scheme 1**. Poly(*δ*-decanolactone) (PDL) is an

amorphous, rubbery, aliphatic polyester that can be synthesized from plant-derived lactone monomers. The "hard moiety-*b*-soft moiety-*b*-hard moiety" ABA-type triblock architecture is important because it endows the BCPs with elastomer-like properties characteristic of the well-known styrene-based thermoplastic elastomers. In fact, our group recently reported completely bio-based elastomers consisting of a maltooligosaccharide as the hard segment and PDL as the soft segment.[14] Importantly, X-ray scattering experiments and atomic force microscopy revealed that the AcCel$_n$-*b*-PDL-*b*-AcCel$_n$s are more likely to microphase-separate compared to their amylose counterparts. Furthermore, we found that the AcCel$_n$-*b*-PDL-*b*-AcCel$_n$s have significantly superior mechanical properties compared to the AcMal$_n$-*b*-PDL-*b*-AcMal$_n$s, in terms of Young's moduli, elongations at break, and toughnesses.

Scheme 1. Syntheses of AcCel$_n$-*b*-PDL-*b*-AcCel$_n$ and AcMal$_n$-*b*-PDL-*b*-AcMal$_n$

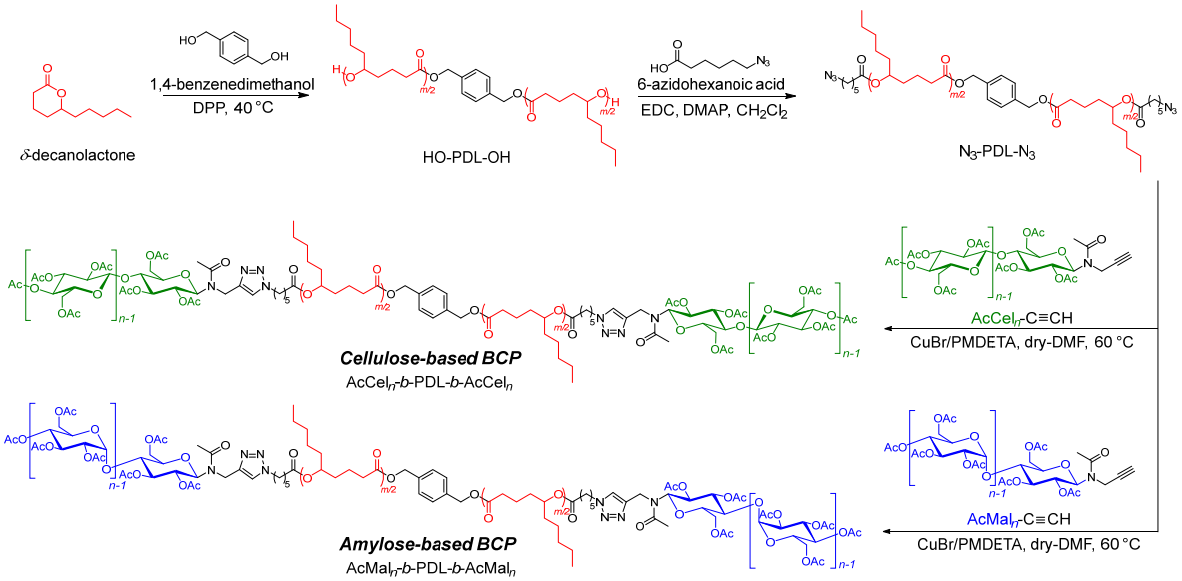

Results and Discussion

Preparation of propargyl-functionalized cellooligosaccharide triacetate and maltooligosaccharide triacetate

We initially synthesized propargyl-functionalized cellooligosaccharide triacetate (AcCel$_n$−C≡CH) and its maltooligosaccharide counterpart (AcMal$_n$−C≡CH). Some researchers reported the syntheses of cellooligosaccharides with different functional groups at the reducing end by the cellodextrin-phosphorylase-mediated (CDP-mediated) oligomerization of *α*-D-glucose-1-phosphase (*α*G1P) (glycosyl donor) in the presence of anomeric *O*-functionalized glucose (primer).[40–44] Inspired by this approach, we envisaged the efficient CDP-mediated synthesis of propargyl-functionalized cellooligosaccharides (Cel$_n$−C≡CH) using propargyl-functionalized primers (**Scheme 2**, upper). In this work, we employed a CDP obtained from *Clostridium thermocellum*. Because His-tagged CDP expressed in *Escherichia coli* BL21(DE3) harbors the pET28a-CDP vector,[45] it was purified by nickel-nitrilotriacetic acid affinity chromatography.[40,45] CDP was obtained at a concentration of 7.7 mg mL^{-1} using the Bradford method. According to previous reports on CDP-mediated cellooligosaccharide syntheses, glucose and cellobiose are known to act as primers.[40,42] Therefore, to identify the optimal primer structure for the preparation of propargyl-functionalized cellooligosaccharides, we examined cellooligosaccharide synthesis using glucose and cellobiose as primers (50 mM) in the presence of CDP (10 mg L^{-1}) and *α*G1P (200 mM) in 4-(2-hydroxyethyl)-1-piperazineethanesulfonic acid (HEPES) buffer solutions (pH = 7.5) at 60 °C for 7 d. Both reactions produced a cellooligosaccharide as a water-insoluble product; however, the yield was significantly higher when cellobiose (~23%) was used as the primer rather than glucose (~4%). Based on these results, we employed *N*-acetyl-propargyl D-(+)-cellobiose (CB−C≡CH; **Figure S1** for ^{1}H NMR and FT-IR spectra) as the primer for the synthesis of

Cel$_n$−C≡CH. The desired product was successfully synthesized in 23.0% yield under the aforementioned conditions using CB−C≡CH as the primer.

Scheme 2. Syntheses of propargyl-functionalized cellooligosaccharide triacetate and maltooligosaccharide triacetate

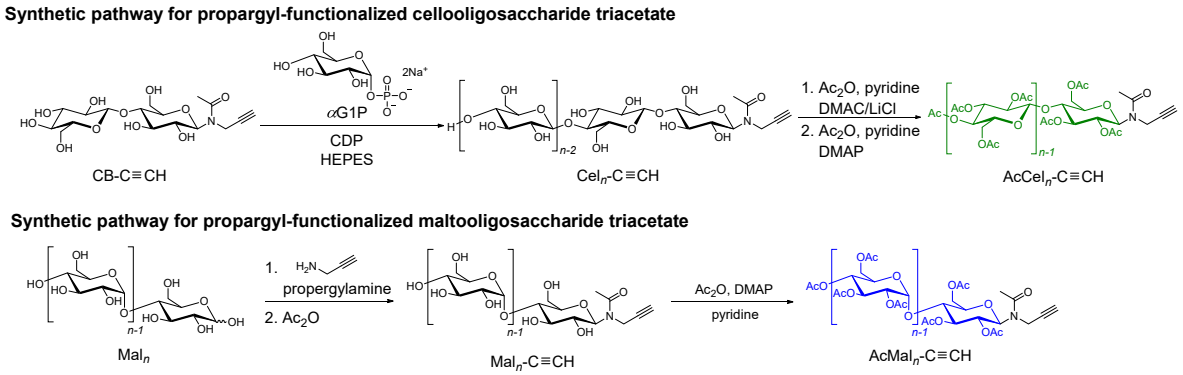

The ^{1}H NMR spectrum of the prepared Cel$_n$−C≡CH exhibited characteristic signals for the proton on the reducing terminal (*1*) at 5.39 and 4.88 ppm, the methine group (*a*) at 2.54 ppm, and the methyl groups (*b*) at 2.30 and 2.23 ppm; these signals were justifiably assigned to the expected structure (**Figure 1** (a), upper). The number-average degree of polymerization of the prepared Cel$_n$−C≡CH was calculated to be 7.19 by integrating and comparing the signals corresponding to the anomeric protons of the reducing terminal (*1*) and repeating units (*1*' and *1*"), which corresponds to a number-averaged molecular weight ($M_{n,NMR}$) of 1,260. The FT-IR spectrum of the product shows a characteristic absorption band at 1,645 cm^{-1} that corresponds to the stretching of the amido C=O group on the anomeric functional group (**Figure S3** (a)). To investigate the structure in detail, the product was subjected to matrix-assisted laser desorption/ionization time-of-flight mass spectrometry (MALDI-TOF MS). The MALDI-TOF mass spectrum shows two series of repeating peaks separated by approximately 162 Da in the 900–1,600 Da range, among

which one series is consistent with the Na^+ adducts, while the other with the K^+ adducts of Cel_n−C≡CH (**Figure S2**). For example, the peak at *m/z* = 1254.4 matches the theoretical molecular mass for the Na^+ adduct of the 7-mer in Cel_n−C≡CH ($[M + Na]^+$ = 1254.4 Da). The synthesized Cel_n−C≡CH mainly comprises 6- to 8-mers according to the MALDI-TOF mass spectrum. The number-average molecular weight was determined by MALDI-TOF MS ($M_{n,MALDI}$) to be 1,190, which is in good agreement with the $M_{n,NMR}$ value (1,230).

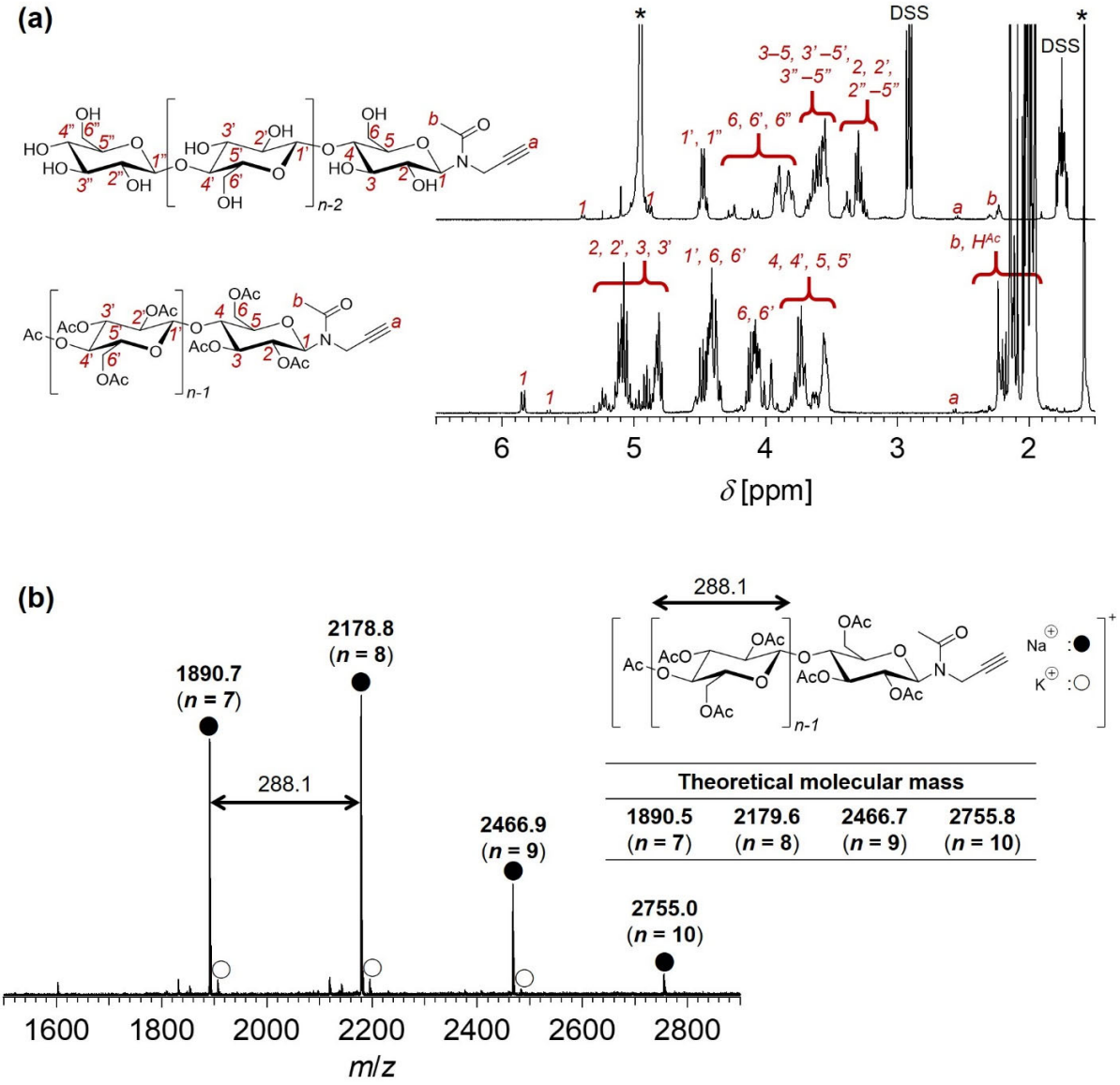

Figure 1. Characterization of Cel_n−C≡CH and $AcCel_n$−C≡CH. (a) ^{1}H NMR spectra of Cel_n−C≡CH (upper) in D_2O containing sodium trimethylsilylpropanesulfonate (DSS) and 10% (w/w) NaOD and $AcCel_n$−C≡CH in $CDCl_3$ (lower) (400 MHz). (b) MALDI-TOF mass spectrum and theoretical molecular masses of $AcCel_n$−C≡CH.

The prepared Cel$_n$−C≡CH was subsequently subjected to acetylation following solvent-exchange with H_2O, acetone, and *N*,*N*-dimethylacetamide (DMAc). Acetylation was carried out using Ac_2O and pyridine in LiCl/DMAc for 5 d.[46] However, ^{1}H NMR and FT-IR spectroscopy of the product revealed incomplete acetylation. Therefore, the partially acetylated product was further treated with Ac_2O and pyridine in the presence of 4-(dimethylamino)pyridine (DMAP) to ensure complete acetylation. The ^{1}H NMR spectrum of the final product exhibited the characteristic signals of the acetyl groups (**Figure 1** (a), lower). The number-average degree of polymerization of the prepared AcCel$_n$−C≡CH was calculated to be 6.76 by integrating and comparing the signals corresponding to the anomeric protons of the reducing terminal (*1*) and repeating units (*2*, *2'*, *3*, and *3'*), which corresponds to a $M_{n,NMR}$ of 2,090. The FT-IR spectrum of the product lacks the absorption band attributable to the hydroxyl groups and exhibits new absorption bands attributable to ester bonds (**Figure S3** (a)). The MALDI-TOF mass spectrum exhibited two series of repeated peaks in the 1,800–3,000 Da range separated by approximately 288 Da, which correspond to the repeating unit of AcCel$_n$−C≡CH (**Figure 1** (b)). These spectroscopic results quantitatively confirmed that all hydroxyl groups of Cel$_n$−C≡CH had been acetylated. The size exclusion chromatography (SEC) trace of AcCel$_n$−C≡CH exhibited a monomodal peak and a narrow dispersity ($Đ$ = 1.06), and the SEC-based number-average molecular weight ($M_{n,SEC}$) was calculated to be 2,080 when calibrated against a polystyrene standard (**Figure S3** (b)). In summary, we successfully prepared a well-defined and perfectly acetylated AcCel$_n$−C≡CH with an average DP of 6.76.

AcMal$_n$−C≡CH, which is the amylose counterpart of AcCel$_n$−C≡CH, was successfully prepared in three steps (**Scheme 2**, lower). According to a previously reported procedure,[47] a commercially available maltooligosaccharide was treated with propargyl amine in the absence of

a solvent followed by Ac_2O in MeOH, to produce propargyl-functionalized maltooligosaccharide (Mal_n−C≡CH). Subsequent *O*-acetylation with Ac_2O in the presence of DMAP in pyridine produced $AcMal_n$−C≡CH, which mainly comprises 6- to 8-mers according to MALDI-TOF MS. The $M_{n,NMR}$ and $Đ$ values of the prepared $AcMal_n$−C≡CH were determined to be 2,020 (DP = 6.51) and 1.09, respectively, according to ^{1}H NMR spectroscopy and SEC (see **Figures S4** and **S5** for more details).

Triblock copolymer synthesis

Ring-opening polymerization (ROP) of *δ*-decanolactone was carried at 40 °C using diphenyl phosphate (DPP) and 1,4-benzenedimethanol (BDM) as the catalyst and initiator, respectively, according the procedure reported previously by us, to produce poly(*δ*-decanolactone) diol (HO–PDL–OH) as the central soft segment of the target triblock copolymer.[14] In this work, PDLs with three molecular weights were synthesized by varying the initial monomer-to-initiator ratio (HO–PDL_{6k}–OH, $M_{n,\,NMR}$ = 5,590, $Đ$ = 1.07; HO–PDL_{10k}–OH, $M_{n,\,NMR}$ = 10,000, $Đ$ = 1.06; HO–PDL_{22k}–OH, $M_{n,\,NMR}$ = 21,600, $Đ$ = 1.06). The HO–PDL–OH groups were thereafter treated with 6-azidohexanoic acid (N_3–COOH) to give the corresponding *α*,*ω*-diazido-functionalized PDLs (N_3–PDL_{6k}–N_3, $M_{n,NMR}$ = 5,900, $Đ$ = 1.07; N_3–PDL_{10k}–N_3, $M_{n,NMR}$ = 10,300, $Đ$ = 1.06; N_3–PDL_{22k}–N_3, $M_{n,NMR}$ = 21,900, $Đ$ = 1.09; **Figures S6–S8** show the ^{1}H NMR spectra of the HO–PDL–OHs and N_3–PDL–N_3s).

Finally, the copper-catalyzed azido-alkyne click reactions between the prepared N_3–PDL–N_3s and $AcCel_n$−C≡CH or $AcMal_n$−C≡CH were carried out in DMF using CuBr/PMDETA as the catalyst to produce the target ABA-type triblock BCPs, namely, $AcCel_n$-*b*-PDL_{6k}-*b*-$AcCel_n$,

AcCel$_n$-*b*-PDL$_{10k}$-*b*-AcCel$_n$, AcCel$_n$-*b*-PDL$_{22k}$-*b*-AcCel$_n$, AcMal$_n$-*b*-PDL$_{6k}$-*b*-AcMal$_n$, AcMal$_n$-*b*-PDL$_{10k}$-*b*-AcMal$_n$, and AcMal$_n$-*b*-PDL$_{22k}$-*b*-AcMal$_n$, in isolated yields of 26%–80%. The FT-IR spectra of the products confirmed the disappearance of the absorption band at approximately 2,100 cm^{-1} attributable to azido groups (**Figures S9–14** (b)), and each SEC elution peak appeared in a higher molecular weight region compared to the azido-functionalized PDL peak, which suggests that each click reaction proceeded quantitatively (**Figure 2**). Furthermore, the ^{1}H NMR spectra exhibit signals derived from the PDL and AcCel$_n$ or AcMal$_n$ segments that are assigned to the expected chemical structures, thereby confirming that the AcCel$_n$-*b*-PDL-*b*-AcCel$_n$s and AcMal$_n$-*b*-PDL-*b*-AcMal$_n$s had been successfully synthesized (**Figures S9−S14** (a)). The molecular weights, *Đ* values, and volume fractions of the PDL segments (f_{PDL}) of the prepared AcCel$_n$-*b*-PDL-*b*-AcCel$_n$s and AcMal$_n$-*b*-PDL-*b*-AcMal$_n$s are summarized in **Table 1**.

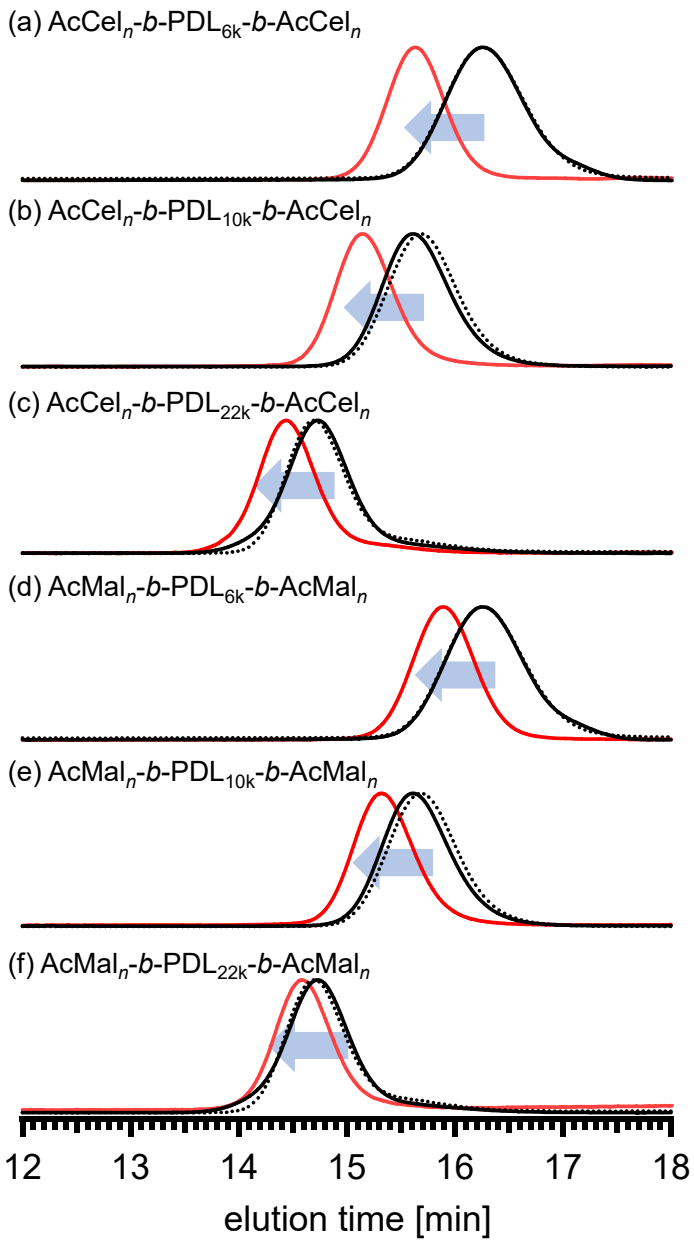

Figure 2. SEC traces of (a) AcCel$_n$-*b*-PDL$_{6k}$-*b*-AcCel$_n$, (b) AcCel$_n$-*b*-PDL$_{10k}$-*b*-AcCel$_n$, (c) AcCel$_n$-*b*-PDL$_{22k}$-*b*-AcCel$_n$, (d) AcMal$_n$-*b*-PDL$_{6k}$-*b*-AcMal$_n$, (e) AcMal$_n$-*b*-PDL$_{10k}$-*b*-AcMal$_n$, and (f) AcMal$_n$-*b*-PDL$_{22k}$-*b*-AcMal$_n$ (eluent, THF; flow rate, 1.0 mL min^{-1}). The solid red, solid black, and dotted black lines represent the BCPs and their corresponding N_3–PDL–N_3 and HO–PDL–OH units, respectively.

Table 1. Molecular characteristics of AcCel$_n$-*b*-PDL-*b*-AcCel$_n$s and AcMal$_n$-*b*-PDL-*b*-AcMal$_n$s

Polymer	M_n	$Đ^c$	$T_{g,PDL}{}^d$ [°C]	$T_{g,Cel}{}^d$ [°C]	$T_{m,Cel}{}^d$ [°C]	$T_{g,Mal}{}^d$ [°C]	$f_{PDL}{}^e$
AcCel$_n$−C≡CH	2,090[a]	1.06	-	110	167	-	-
AcMal$_n$−C≡CH	2,020[a]	1.09	-	-	-	101	-
AcCel$_n$-*b*-PDL$_{6k}$-*b*-AcCel$_n$	10,100[b]	1.04	−52	86	-	-	0.65
AcCel$_n$-*b*-PDL$_{10k}$-*b*-AcCel$_n$	14,500[b]	1.04	−52	97	162	-	0.77
AcCel$_n$-*b*-PDL$_{22k}$-*b*-AcCel$_n$	26,100[b]	1.06	−53	106	-	-	0.87
AcMal$_n$-*b*-PDL$_{6k}$-*b*-AcMal$_n$	9,900[b]	1.04	−52	-	-	60	0.64
AcMal$_n$-*b*-PDL$_{10k}$-*b*-AcMal$_n$	14,300[b]	1.04	−51	-	-	60	0.76
AcMal$_n$-*b*-PDL$_{22k}$-*b*-AcMal$_n$	25,900[b]	1.04	−54	-	-	55	0.87

[a]Determined by ^{1}H NMR spectroscopy in $CDCl_3$. [b]Calculated from the molecular weight of AcCel$_n$−C≡CH or AcMal$_n$−C≡CH determined by MALDI-TOF and the molecular weight of the corresponding N_3–PDL–N_3 determined by ^{1}H NMR spectroscopy in $CDCl_3$. [c]Determined by SEC in THF using polystyrene standards. [d]Determined by DSC at a heating rate of 10 °C min^{-1}. [e]Calculated using the density of each block: 1.29 g cm^{-3} for AcCel$_n$−C≡CH,[48] 1.20 g cm^{-3} for AcMal$_n$−C≡CH,[49] and 0.97 g cm^{-3} for PDL.[50]

Thermal properties

To gain fundamental insight into the differences in the physical properties originating from the oligosaccharide blocks, we initially evaluated the thermal properties of the AcCel$_n$-*b*-PDL-*b*-AcCel$_n$s and AcMal$_n$-*b*-PDL-*b*-AcMal$_n$s by thermogravimetric analysis (TGA) and differential scanning calorimetry (DSC) in a nitrogen atmosphere. According to the TGA data, all of the studied BCP samples were thermally stable up to approximately 280 °C and exhibited 5% weight-loss temperatures ($T_{d5\%}$) in the 290–320 °C range (**Figures S15** and **S16**). Visual inspection during TGA revealed that all BCP samples changed their appearance; they transformed from a solid to a

melt state close to the glass transition temperature of the AcCel$_n$ or AcMal$_n$ segment, consistent with thermoplastic behavior. The DSC curves of the AcCel$_n$-*b*-PDL-*b*-AcCel$_n$s and AcMal$_n$-*b*-PDL-*b*-AcMal$_n$s acquired during the second heating process exhibited two baseline shifts derived from the glass transitions of the PDL and AcCel$_n$ or AcMal$_n$ segments (**Figure 3**). The glass transition temperatures of the PDL ($T_{g,PDL}$), AcCel$_n$ ($T_{g,Cel}$), and AcMal$_n$ segments ($T_{g,Mal}$) are approximately −50, 95, and 60 °C, respectively (**Figures 3** and **S17**). The fact that $T_{g,PDL}$ and $T_{g,Cel}$ (or $T_{g,Mal}$) were observed separately indicates phase separation between the PDL and AcCel$_n$ (or AcMal$_n$) segments. The $T_{g,Mal}$ values of the AcMal$_n$-*b*-PDL-*b*-AcMal$_n$s were considerably lower than that of AcMal$_n$–C≡CH, which indicates partial mixing of the AcMal$_n$ and PDL domains. Similarly, partial mixing of the AcCel$_n$ and PDL domains resulted in lower $T_{g,Cel}$ values for the AcCel$_n$-*b*-PDL-*b*-AcCel$_n$s than AcCel$_n$–C≡CH. Interestingly, $T_{g,Cel}$ was observed to increase with increasing f_{PDL}, which is attributable to increasing segregation strength associated with increasing AcCel$_n$-*b*-PDL-*b*-AcCel$_n$ total molecular weight. Notably, the DSC curve of AcCel$_n$-*b*-PDL$_{10k}$-*b*-AcCel$_n$ exhibited a small endothermic peak at 163 °C due to the melting of the AcCel$_n$ segment ($T_{m,Cel}$), which indicates that the BCP is semi-crystalline in nature. The DSC trace of AcCel$_n$−C≡CH clearly exhibits a $T_{m,Cel}$ at 167 °C; however, the traces for AcCel$_n$-*b*-PDL$_{6k}$-*b*-AcCel$_n$ and AcCel$_n$-*b*-PDL$_{22k}$-*b*-AcCel$_n$ did not exhibit any melting peaks. Given the small area of the melting transition of the AcCel$_n$ segment in AcCel$_n$-*b*-PDL$_{10k}$-*b*-AcCel$_n$, crystallization tends to occur slowly. In contrast, the AcMal$_n$-*b*-PDL-*b*-AcMal$_n$s and AcMal$_n$−C≡CH did not exhibit any melting transition, which confirms the amorphous nature of the AcMal$_n$ segment.

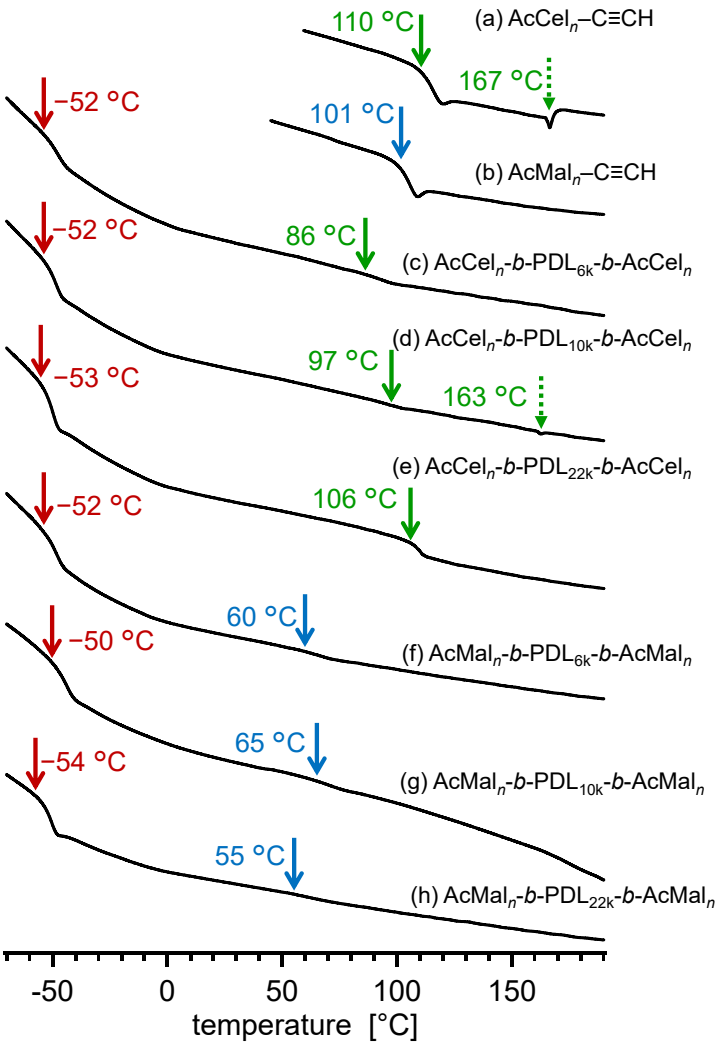

Figure 3. DSC curves of (a) AcCel$_n$–C≡CH, (b) AcMal$_n$–C≡CH, (c) AcCel$_n$-*b*-PDL$_{6k}$-*b*-AcCel$_n$, (d) AcCel$_n$-*b*-PDL$_{10k}$-*b*-AcCel$_n$, (e) AcCel$_n$-*b*-PDL$_{22k}$-*b*-AcCel$_n$, (f) AcMal$_n$-*b*-PDL$_{6k}$-*b*-AcMal$_n$, (g) AcMal$_n$-*b*-PDL$_{10k}$-*b*-AcMal$_n$, and (h) AcMal$_n$-*b*-PDL$_{22k}$-*b*-AcMal$_n$ during the second heating run (heating rate: 10 °C min^{-1}).

Microphase-separated structures

To investigate the impact of the oligosaccharide segments on the BCP self-assembly behavior, the microphase-separated structures of the AcCel$_n$-*b*-PDL-*b*-AcCel$_n$s and AcMal$_n$-*b*-PDL-*b*-AcMal$_n$s were investigated through small-angle X-ray scattering (SAXS) experiments on bulk samples, which were prepared by casting toluene solutions of the BCPs, followed by drying for 15 h at atmospheric pressure and for 1 d under vacuum at room temperature. The prepared films were subsequently thermally annealed under vacuum at 130 °C for 6 or 24 h.

The SAXS profiles of the non-annealed AcCel$_n$-*b*-PDL-*b*-AcCel$_n$s and AcMal$_n$-*b*-PDL-*b*-AcMal$_n$s exhibited only primary peaks indicative of weak segregation between the PDL and acetyl oligosaccharide segments with no periodically ordered structures (**Figure 4**). The mean distance between the phase-separated microdomains was calculated to be approximately 10 nm based on the Bragg equation using the position of the primary peak (q^*). In contrast, dramatic differences were observed in the microphase-separated structures of the AcCel$_n$-*b*-PDL-*b*-AcCel$_n$s and AcMal$_n$-*b*-PDL-*b*-AcMal$_n$s upon thermal annealing. The SAXS profiles of the AcMal$_n$-*b*-PDL-*b*-AcMal$_n$s exhibited only primary peaks, regardless of the annealing conditions, which implies that these BCPs do not meet the requirements for ordered microphase-separation. In contrast, the SAXS profiles of the AcCel$_n$-*b*-PDL-*b*-AcCel$_n$s exhibited primary peaks and additional higher-order scattering peaks upon thermal annealing at 130 °C for appropriate durations. The SAXS profile of AcCel$_n$-*b*-PDL$_{6k}$-*b*-AcCel$_n$ exhibited a higher-order scattering peak at $3q^*$ in addition to q^*, indicative of a lamellar (LAM) structure (**Figure 4** (a)); no even-ordered peak appeared in this SAXS profile, which indicates that the volumes of the AcCel$_n$ and PDL microdomains are nearly equal.[51] The SAXS profiles of AcCel$_n$-*b*-PDL$_{10k}$-*b*-AcCel$_n$ and AcCel$_n$-*b*-PDL$_{22k}$-*b*-AcCel$_n$ also exhibited higher-order scattering peaks at $\sqrt{3}q^*$, $2q^*$, $\sqrt{7}q^*$, and $3q^*$, and $\sqrt{2}q^*$, $\sqrt{3}q^*$, $\sqrt{5}q^*$, and $\sqrt{7}q^*$,

indicative of hexagonal cylindrical (HEX) and body-centered cubic (BCC) spherical structures, respectively (**Figure 4** (c) and (e), respectively). The domain-spacing (*d*) of the thermally annealed AcCel$_n$-*b*-PDL$_{6k}$-*b*-AcCel$_n$, AcCel$_n$-*b*-PDL$_{10k}$-*b*-AcCel$_n$, and AcCel$_n$-*b*-PDL$_{22k}$-*b*-AcCel$_n$ were determined to be 9.6, 10.3, and 12.1 nm, respectively; the *d* value increases with increasing molecular weight. Overall, the AcCel$_n$-*b*-PDL-*b*-AcCel$_n$s are more likely to undergo ordered microphase-separation than the AcMal$_n$-*b*-PDL-*b*-AcMal$_n$s, despite being composed of the same monomeric units and possessing comparable chemical compositions. This is partly attributable to the rigidity granted to the AcCel$_n$ segments by their *β*-1,4-linked cellulose backbone. The longer Kuhn and persistence lengths of cellulose compared to those of amylose[13,52,53] induce microphase-separation in the AcCel$_n$-*b*-PDL-*b*-AcCel$_n$s. The fact that AcCel$_n$–C≡CH has a larger $M_{n,SEC}$ than AcMal$_n$–C≡CH, despite their comparable $M_{n,NMR}$ values, implies that the AcCel$_n$ segment is more rigid than AcMal$_n$. In addition, the AcCel$_n$ segment exhibited the potential to crystallize, as revealed by DSC, which indicates its stronger tendency to self-aggregate. The wide-angle X-ray diffraction (WAXD) data also confirmed that the AcCel$_n$ segment is crystalline in nature (**Figures S18** and **S19**). While the WAXD profile of AcMal$_n$–C≡CH and the AcMal$_n$-*b*-PDL-*b*-AcMal$_n$s showed only amorphous halos, AcCel$_n$–C≡CH and the AcCel$_n$-*b*-PDL-*b*-AcCel$_n$s showed diffraction peaks assignable to cellulose triacetate I crystals.[54,55] This may further enhance microphase-separation in the AcCel$_n$-*b*-PDL-*b*-AcCel$_n$s and significantly alter the self-assembly properties of the AcCel$_n$-*b*-PDL-*b*-AcCel$_n$s and AcMal$_n$-*b*-PDL-*b*-AcMal$_n$s.

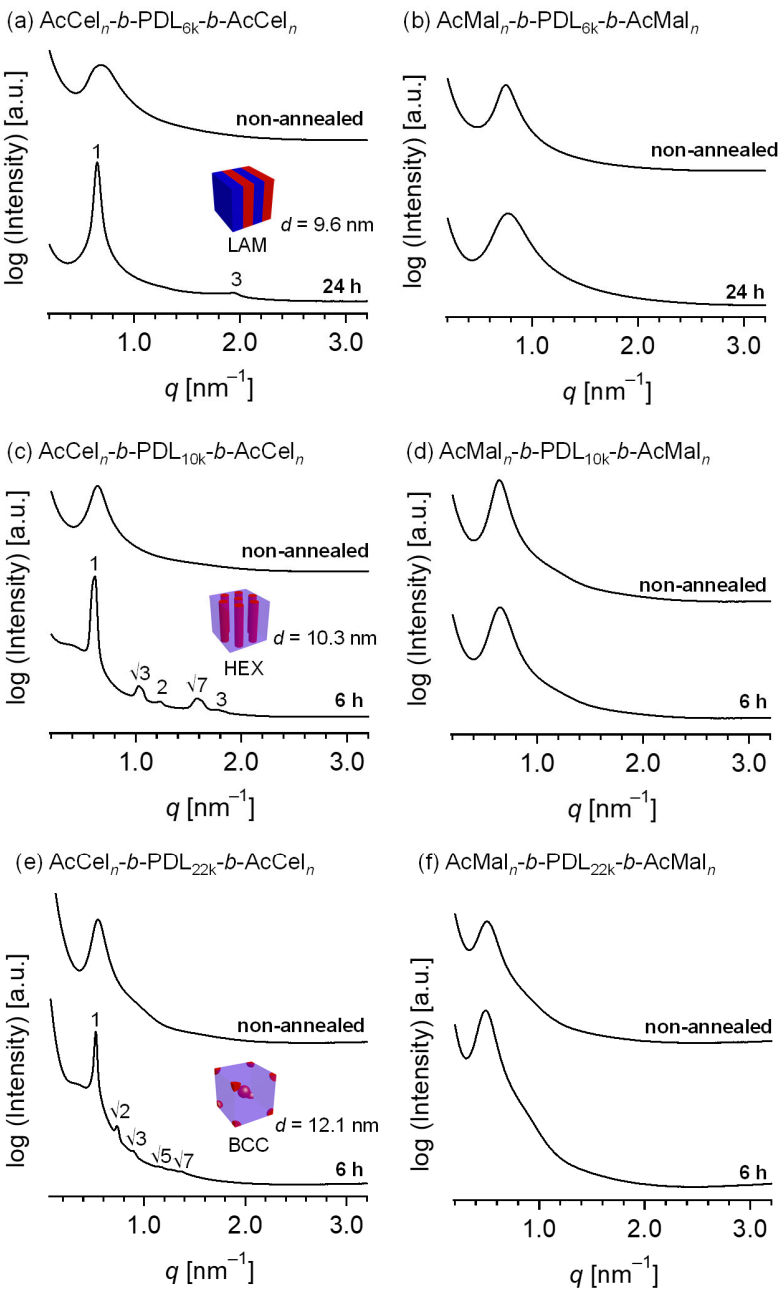

Figure 4. SAXS profiles of (a) AcCel$_n$-*b*-PDL$_{6k}$-*b*-AcCel$_n$, (b) AcMal$_n$-*b*-PDL$_{6k}$-*b*-AcMal$_n$, (c) AcCel$_n$-*b*-PDL$_{10k}$-*b*-AcCel$_n$, (d) AcMal$_n$-*b*-PDL$_{10k}$-*b*-AcMal$_n$, (e) AcCel$_n$-*b*-PDL$_{22k}$-*b*-AcCel$_n$, and (f) AcMal$_n$-*b*-PDL$_{22k}$-*b*-AcMal$_n$ without thermal annealing and after annealing at 130 °C for 6 or 24 h.

To further investigate the microphase-separation behavior, we subjected BCP thin films to atomic force microscopy (AFM) (**Figure S20**); the thin-film samples were prepared by spin-coating 1% (w/w) solutions of AcCel$_n$-*b*-PDL-*b*-AcCel$_n$s and AcMal$_n$-*b*-PDL-*b*-AcMal$_n$s in toluene onto bare Si substrates. The AFM phase images of the non-annealed AcCel$_n$-*b*-PDL$_{6k}$-*b*-AcCel$_n$, AcCel$_n$-*b*-PDL$_{10k}$-*b*-AcCel$_n$, AcMal$_n$-*b*-PDL$_{6k}$-*b*-AcMal$_n$, and AcMal$_n$-*b*-PDL$_{10k}$-*b*-AcMal$_n$ thin films show less-ordered fingerprint patterns. In contrast, the non-annealed AcCel$_n$-*b*-PDL$_{22k}$-*b*-AcCel$_n$ and AcMal$_n$-*b*-PDL$_{22k}$-*b*-AcMal$_n$ thin films show less-ordered spheres. These results are consistent with the fact that featureless SAXS profiles were observed for the non-annealed samples in the bulk. The morphologies of the AcCel$_n$-*b*-PDL-*b*-AcCel$_n$s were significantly altered by thermal annealing in the thin-film and bulk states. The AFM phase image of the AcCel$_n$-*b*-PDL$_{6k}$-*b*-AcCel$_n$ thin film showed a peculiar morphology consisting of rectangular units, which are related to the crystallization of the AcCel$_n$ segment.[56] A highly ordered fingerprint-like pattern was observed in the thermally annealed AcCel$_n$-*b*-PDL$_{10k}$-*b*-AcCel$_n$ thin film, which is attributable to the horizontally orientated HEX structure, considering the bulk SAXS result. The spherical structures observed in the thermally annealed AcCel$_n$-*b*-PDL$_{22k}$-*b*-AcCel$_n$ are attributable to the BCC spherical structure. The AFM images of AcCel$_n$-*b*-PDL$_{10k}$-*b*-AcCel$_n$ and AcCel$_n$-*b*-PDL$_{22k}$-*b*-AcCel$_n$ revealed the *d* values of 10.8 and 12.0 nm, respectively, which were in good agreement with the values derived from the bulk SAXS results. As expected from the bulk SAXS results, the AcMal$_n$-*b*-PDL-*b*-AcMal$_n$ thin films did not exhibit any ordered patterns following thermal annealing, which verifies that the cellulose-based BCPs are more likely to microphase-separate than their amylose counterparts.

Mechanical properties

Finally, to investigate the impact of the hard oligosaccharide segment on mechanical properties, dog-bone-shaped specimens of solvent-cast BCPs were subjected to tensile testing. Note that it was difficult to subject AcMal$_n$-*b*-PDL$_{22k}$-*b*-AcMal$_n$ to tensile testing because it is a sticky material. The other BCPs exhibited elastic properties, which confirms that the hard microphase-separated oligosaccharide domains act as physical crosslinks between the rubbery PDL chains. The stress–strain curves and key mechanical properties (Young's modulus (E), strain at break (ε_b), stress at break (σ_b), and toughness, and their average values and standard deviations) of the BCP specimens are shown in **Figure 5** and **Table 2**, respectively.

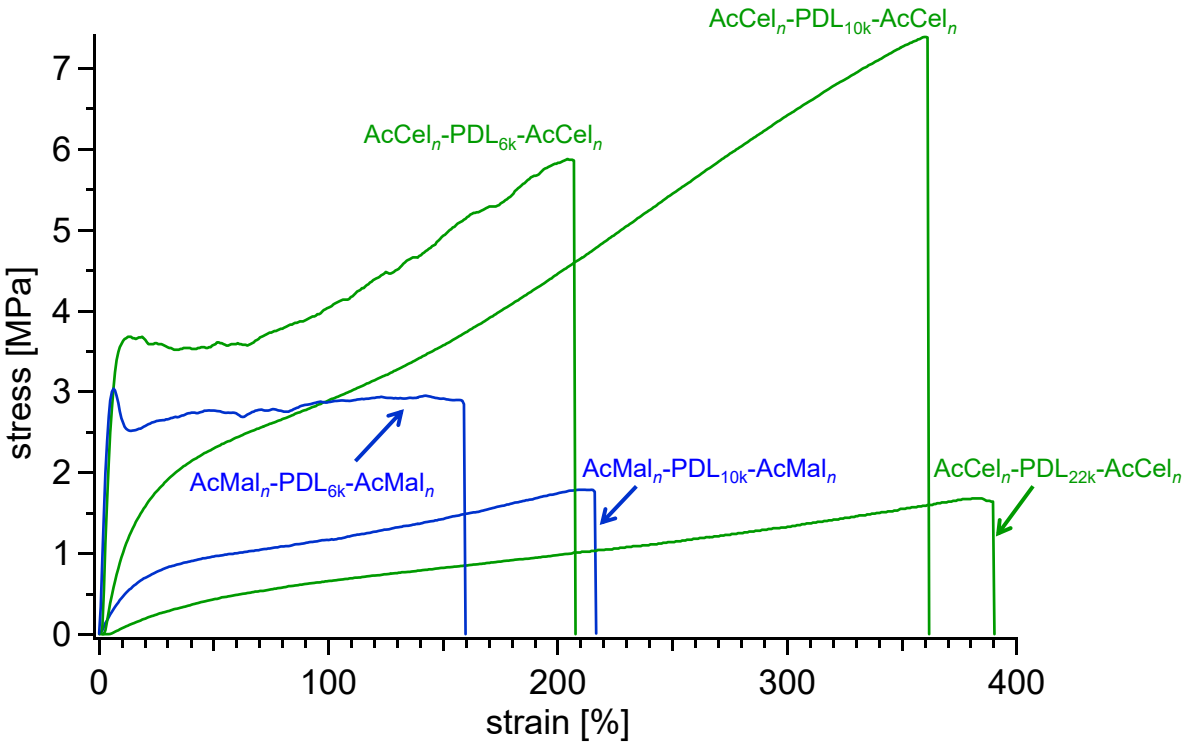

Figure 5. Typical stress–strain curves of the AcCel$_n$-*b*-PDL$_{6k}$-*b*-AcCel$_n$, AcCel$_n$-*b*-PDL$_{10k}$-*b*-AcCel$_n$, AcCel$_n$-*b*-PDL$_{22k}$-*b*-AcCel$_n$, AcMal$_n$-*b*-PDL$_{6k}$-*b*-AcMal$_n$, and AcMal$_n$-*b*-PDL$_{10k}$-*b*-AcMal$_n$ specimens (crosshead speed: 10 mm min^{-1}).

Table 2. Tensile properties of the BCP specimens[a]

BCP	E^a [MPa]	$\varepsilon_b{}^a$ [%]	$\sigma_b{}^a$ [MPa]	Toughness[a] [MJ m^{-3}]
AcCel$_n$-*b*-PDL$_{6k}$-*b*-AcCel$_n$	69±5.1	209±17.6	5.8±0.082	8.9±0.90
AcCel$_n$-*b*-PDL$_{10k}$-*b*-AcCel$_n$	13±1.7	356±8.99	7.1±0.47	15±1.2
AcCel$_n$-*b*-PDL$_{22k}$-*b*-AcCel$_n$	1.3±0.062	385±16.0	1.7±0.047	3.8±0.17
AcMal$_n$-*b*-PDL$_{6k}$-*b*-AcMal$_n$	61±6.8	150±14.6	2.8±0.12	4.2±0.48
AcMal$_n$-*b*-PDL$_{10k}$-*b*-AcMal$_n$	5.6±0.68	198±13.6	1.6±0.14	2.2±0.29

[a]Tensile properties are shown as average values (with standard deviations) for three specimens.

The stress–strain curves show that AcCel$_n$-*b*-PDL$_{6k}$-*b*-AcCel$_n$ and AcMal$_n$-*b*-PDL$_{6k}$-*b*-AcMal$_n$, which possess the lowest f_{PDL} values, exhibit yield points, suggestive of plastic-like behavior irrespective of the type of hard segment. In contrast, AcCel$_n$-*b*-PDL$_{10k}$-*b*-AcCel$_n$, AcCel$_n$-*b*-PDL$_{22k}$-*b*-AcCel$_n$, and AcMal$_n$-*b*-PDL$_{10k}$-*b*-AcMal$_n$ did not exhibit clear yield points, suggesting that BCPs with longer PDL segments exhibit elastomer-like behavior, which is supported by the results of cyclic tensile testing (**Figure S21**), which suggest that the areas enclosed by hysteresis loops, which correlate with the level of plastic deformation, diminish with increasing f_{PDL}. No obvious residual strain was observed following five loading/unloading cycles for AcCel$_n$-*b*-PDL$_{22k}$-*b*-AcCel$_n$, confirming its high level of elastic recovery. A general trend in which ε_b increases and E decreases with increasing f_{PDL} was observed; for example, the ε_b value of AcCel$_n$-*b*-PDL$_{22k}$-*b*-AcCel$_n$ was 1.8-times higher than that of AcCel$_n$-*b*-PDL$_{6k}$-*b*-AcCel$_n$, and the E value of AcCel$_n$-*b*-PDL$_{6k}$-*b*-AcCel$_n$ was 53-times higher than that of AcCel$_n$-*b*-PDL$_{22k}$-*b*-AcCel$_n$. This trend was observed when the ε_b and E values for AcMal$_n$-*b*-PDL$_{6k}$-*b*-AcMal$_n$ and AcMal$_n$-*b*-PDL$_{10k}$-*b*-AcMal$_n$ were compared.

The BCPs containing AcCel$_n$ segments possess significantly superior mechanical properties to those containing AcMal$_n$ segments, despite their comparable molecular weights and chemical compositions. Specifically, the E, ε_b, σ_b, and toughness values of AcCel$_n$-*b*-PDL$_{10k}$-*b*-AcCel$_n$ were 2.3-, 1.8-, 4.4-, and 6.8-times greater than those of AcMal$_n$-*b*-PDL$_{10k}$-*b*-AcMal$_n$, respectively. Furthermore, stress on the AcCel$_n$-*b*-PDL$_{6k}$-*b*-AcCel$_n$ specimen gradually increased beyond the yield point, while AcMal$_n$-*b*-PDL$_{6k}$-*b*-AcMal$_n$ maintained constant stress beyond the yield point until rupture. AcCel$_n$-*b*-PDL-*b*-AcCel$_n$ strain hardening reveals that cellulosic hard-segment pull-out was more effectively hindered in these polymers compared to that in their amylose counterparts.[57] The stronger crosslinking ability of the AcCel$_n$ segment is partly attributable to its crystalline nature, in contrast to the amorphous nature of AcMal$_n$. X-ray crystallography previously revealed that cellulose triacetate and amylose triacetate adopt sheet and helix conformations, respectively.[48,49,58,59] Evidently, the sheet-like conformation is preferred for creating larger interchain attractive forces, which may be responsible for the stronger crosslinking of the AcCel$_n$ segment. In addition, the higher potential to form ordered microphase-separated structures seems to be another important factor that contributes to the superior mechanical performance of the AcCel$_n$-*b*-PDL-*b*-AcCel$_n$s.

Figure S22 compares σ_b and E of AcCel$_n$-*b*-PDL$_{6k}$-*b*-AcCel$_n$, AcCel$_n$-*b*-PDL$_{10k}$-*b*-AcCel$_n$, AcCel$_n$-*b*-PDL$_{22k}$-*b*-AcCel$_n$, AcMal$_n$-*b*-PDL$_{6k}$-*b*-AcMal$_n$, and AcMal$_n$-*b*-PDL$_{10k}$-*b*-AcMal$_n$ with those of commercial thermoplastic elastomers (TPEs). Notably, the E value of AcCel$_n$-*b*-PDL$_{10k}$-*b*-AcCel$_n$ was comparable to or even higher than those of commercial TPEs, such as melt-processable rubber and TPEs containing polyamide hard blocks. The σ_b of AcCel$_n$-PDL$_{10k}$-*b*-AcCel$_n$ was also comparable to those of commercial TPEs, such as melt-processable rubber and

silicone TPEs. This comparison highlights the potential of the AcCel$_n$-*b*-PDL-*b*-AcCel$_n$s as fully bio-based high-performance elastomers.

Conclusions

In this work, novel cellulose-based BCPs (AcCel$_n$-*b*-PDL-*b*-AcCel$_n$s) and their amylose counterparts (AcMal$_n$-*b*-PDL-*b*-AcMal$_n$s) were precisely synthesized. The AcCel$_n$-*b*-PDL-*b*-AcCel$_n$s were found to be more likely to self-assemble than the AcMal$_n$-*b*-PDL-*b*-AcMal$_n$s in their bulk and thin-film states. Because these BCPs have comparable chemical compositions and molecular weights, the dramatic difference in their self-assembly behavior stems from the differences in the types of bonding (i.e., β-1,4 or α-1,4 linkages) in their oligosaccharide segments. More interestingly, the AcCel$_n$-*b*-PDL-*b*-AcCel$_n$s exhibit superior mechanical properties than the AcMal$_n$-*b*-PDL-*b*-AcMal$_n$s, which indicates that stronger physical crosslinking was achieved in the AcCel$_n$ segments. In addition, the Young's modulus (~69 MPa) and elongation at break (~5.8 MPa) of the AcCel$_n$-*b*-PDL-*b*-AcCel$_n$s were comparable to or higher than those of commercially available TPEs. To the best of our knowledge, this is the first report that investigates in detail how small differences in the primary structures of oligosaccharide segments (i.e., α-1,4 or β-1,4 linkages) affect the microphase-separation and mechanical properties of carbohydrate-based BCPs. Overall, we verified the applicability of cellulose-based BCPs exhibit as bio-based and sustainable polymeric materials. Encouraged by these promising results, we are currently working toward the syntheses of bio-based plastics, elastomers, and fibers that possess sufficiently high strengths and toughnesses for practical use by either optimizing the degree of substitution on the cellulose segment or by introducing other soft middle segments.

ASSOCIATED CONTENT

Supporting Information. Experimental section, comparative NMR and FT-IR spectra of precursors, MALDI-TOF mass spectra, comparative FT-IR spectra of precursors and cellulose-based products, SEC traces of cellulosic products, TGA, DSC, AFM, and cyclic tensile testing results.

Author Contributions

K.T., T.I., and T.S. designed the experiments. S.K. wrote the manuscript. S.K. and Y.T. synthesized and characterized the BCPs and analyzed the X-ray data. N.S. and K.I. constructed the plasmid to express CDP and established the process for preparing CDP. T.Y. contributed to the discussion. The manuscript was written through contributions of all authors. All authors have given approval to the final version of the manuscript.

Funding Sources

This work was financially supported by a JSPS Grant-in-Aid for Scientific Research (B) (No. 19H02549, K.T.; No. 20H02792, I.T.; No. 19H02769, T.S.), the Frontier Chemistry Center (Hokkaido University, T.I.), the Photoexcitonix Project (Hokkaido University, T.S.), the Creative Research Institute (Hokkaido University, T.S.), the Iketani Science and Technology Foundation (T.I.), the Asahi Glass Foundation (T.I.), and Toyota Riken (T.I.).

ACKNOWLEDGMENTS

This work was, in part, performed under the approval of the Photon Factory Program Advisory Committee (Proposal 2017G589 and 2019G579). The authors thank Prof. Hajime Ito, Prof. Kenichiro Matsumoto, and Prof. Tasuku Nakajima (Hokkaido University) for their assistance with AFM, tensile testing, and cyclic tensile testing, respectively. The authors thank Prof. Motomitsu Kitaoka (Niigata University) for kindly providing the pET28a-CDP plasmid. The authors thank the NIHON SHOKUHIN KAKO CO., Ltd, for kindly providing Fujioligo G67.

Reference and Notes

(1) Zhu, Y.; Romain, C.; Williams, C. K. Sustainable polymers from renewable resources. *Nature* **2016**, *540*, 354–362. DOI: 10.1038/nature21001

(2) Esposito, D.; Antonietti, M. Redefining biorefinery: the search for unconventional building blocks for materials. *Chem. Soc. Rev.* **2015**, *44*, 5821–5835. DOI: 10.1039/c4cs00368c

(3) Bozell, J. J.; Petersen, G. R. Technology development for the production of biobasaed products from biorefinery carbohydrates—the US Department of Energy's "Top 10" revisited. *Green Chem*. **2010**, *12*, 539–554. DOI: 10.1039/b922014c

(4) Östmark, E.; Nyström, D.; Malmström, E. Unimolecular Nanocontainers Prepared by ROP and Subsequent ATRP from Hydroxypropylcellulose. *Macromolecules* **2008**, *41*, 4405–4415. DOI: 10.1021/ma702681u

(5) Nouvel, C.; Frochot, C.; Sadtler, V.; Dubois, P.; Dellacherie, E.; Six, J. -L. Polylactide-Grafted Dextrans: Synthesis and Properties at Interfaces and in Solution. *Macromolecules* **2004**, *37*, 4981–4988. DOI: 10.1021/ma049857x

(6) Palumbo, F. S.; Pitarresi, G.; Mandracchia, D.; Tripodo, G.; Giammona, G. New graft copolymers of hyaluronic acid and polylactic acid: Synthesis and characterization. *Carbohydr. Polym.* **2006**, *66*, 379–385. DOI: 10.1016/j.carbpol.2006.03.023

(7) Colinet, I.; Dulong, V.; Hamaide, T.; Le Cerf, D.; Picton, L. New amphiphilic modified polysaccharides with original solution behaviour in salt media. *Carbohydr. Polym.* **2009**, *75*, 454–462. DOI: 10.1016/j.carbpol.2008.08.002

(8) Maruyama, A.; Ishihara, T.; Kim, J. -S.; Kim, S. W.; Akaike, T. Nanoparticle DNA Carrier with Poly(L-Lysine) Grafted Polysaccharide Copolymer and Poly(D,L-Lactic Acid). *Bioconjug. Chem.* **1997**, *8*, 735–742. DOI: 10.1021/bc9701048

(9) Asayama, S.; Nogawa, M.; Takei, Y.; Akaike, T.; Maruyama, A. Synthesis of Novel Polyampholyte Comb-Type Copolymers Consisting of a Poly(L-Lysine) Backbone and Hyaluronic Acid Side Chains for a DNA Carrier. *Bioconjug. Chem.* **1998**, *9*, 476–481. DOI: 10.1021/bc970213m

(10) Aissou, K.; Otsuka, I.; Rochas, C.; Fort, S.; Halila, S.; Borsali, R. Nano-Organization of Amylose-*b*-Polystyrene Block Copolymer Films Doped with Bipyridine. *Langmuir* **2011**, *27*, 4098–4103. DOI: 10.1021/la104936k

(11) Isono, T.; Kawakami, N.; Watanabe, K.; Yoshida, K.; Otsuka, I.; Mamiya, H.; Ito, H.; Yamamoto, T.; Tajima, K.; Borsali, R.; Satoh, T. Microphase separation of carbohydrate-based star-block Copolymers with sub-10 nm periodicity. *Polym. Chem.* **2019**, *10*, 1119–1129. DOI: 10.1039/c8py01745j

(12) Isono, T.; Komaki, R.; Lee, C.; Kawakami, N.; Ree, B. J.; Watanabe, K.; Yoshida, K.; Mamiya, H.; Yamamoto, T.; Borsali, R.; Tajima, K.; Satoh, T. Rapid access to discrete and monodisperse block co-oligomers from sugar and terpenoid toward ultrasmall periodic nanostructures. *Commun. Chem.* **2020**, *3*, 1–9. DOI: 10.1038/s42004-020-00385-y

(13) Schatz, C.; Lecommandoux, S. Polysaccharide-Containing Block Copolymers: Synthesis, Properties and Applications of an Emerging Family of Glycoconjugates. *Macromol. Rapid Commun.* **2010**, *31*, 1664–1684. DOI: 10.1002/marc.201000267

(14) Isono, T.; Nakahira, S.; Hsieh, H. -C.; Katsuhara, S.; Mamiya, H.; Yamamoto, T.; Chen, W. -C.; Borsali, R.; Tajima, K.; Satoh, T. Carbohydrates as Hard Segments for Sustainable Elastomers: Carbohydrates Direct the Self-Assembly and Mechanical Properties of Fully Bio-Based Block Copolymers. *Macromolecules* **2020**, *53*, 5408–5417. DOI: 10.1021/acs.macromol.0c00611

(15) Ikeda, Y.; Nakamura, Y.; Kajiwara, K.; Kohjiya, S. Chemical Modification of Butyl Rubber. III. Butyl Rubber with D-maltose Derivative as Pendant Groups. *J. Polym. Sci. Part A Polym. Chem.* **1995**, *33*, 2657–2665. DOI: 10.1002/pola.1995.080331512

(16) Nasiri, M.; Reineke, T. M. Sustainable glucose-based block copolymers exhibit elastomeric and adhesive behavior. *Polym. Chem.* **2016**, *7*, 5233–5240. DOI: 10.1039/c6py00700g

(17) Katsuhara, S.; Mamiya, H.; Yamamoto, T.; Tajima, K.; Isono, T.; Satoh, T. Metallopolymer-*block*-oligosaccharide for sub-10 nm microphase separation. *Polym. Chem.* **2020**, *11*, 2995–3002. DOI: 10.1039/d0py00271b

(18) Otsuka, I.; Nilsson, N.; Suyatin, D. B.; Maximov, I.; Borsali, R. Carbohydrate-based block copolymer systems: directed self-assembly for nanolithography applications. *Soft Matter* **2017**, *13*, 7406–7411. DOI: 10.1039/c7sm01429e

(19) Cushen, J. D.; Otsuka, I.; Bates, C. M.; Halila, S.; Fort, S.; Rochas, C.; Easley, J. A.; Rausch, E. L.; Thio, A.; Borsali, R.; Willson, C. G.; Ellison, C. J. Oligosaccharide/Silicon-Containing Block Copolymers with 5 nm Features for Lithographic Applications. *ACS Nano* **2012**, *6*, 3424–3433. DOI: 10.1021/nn300459r

(20) Hung, C. -C.; Nakahira, S.; Chiu, Y. -C.; Isono, T.; Wu, H. -C.; Watanabe, K.; Chiang, Y. -C.; Takashima, S.; Borsali, R.; Tung, S. H.; Satoh, T.; Chen, W. -C. Control over Molecular Architectures of Carbohydrate-Based Block Copolymers for Stretchable Electrical Memory Devices. *Macromolecules* **2018**, *51*, 4966–4975. DOI: 10.1021/acs.macromol.8b00874

(21) Chuang, T. -H.; Chiang, Y. -C.; Hsieh, H. -C.; Isono, T.; Huang, C. -W.; Borsali, R.; Satoh, T.; Chen, W. -C. Nanostructure- and Orientation-Controlled Resistive Memory Behaviors of Carbohydrate-*block*-Polystyrene with Different Molecular Weights via Solvent Annealing. *ACS Appl. Mater. Interfaces* **2020**, *12*, 23217–23224. DOI: 10.1021/acsami.0c04551

(22) Sun, H. -S.; Chen, Y.; Lee, W. -Y.; Chiu, Y. -C.; Isono, T.; Satoh, T.; Kakuchi, T.; Chen, W. -C. Synthesis, morphology, and electrical memory application of oligosaccharide-based block copolymers with π-conjugated pyrene moieties and their supramolecules. *Polym. Chem.* **2016**, *7*, 1249–1263. DOI: 10.1039/c5py01697e

(23) Sun, H. -S.; Chiu, Y. -C.; Lee, W. -Y.; Chen, Y.; Hirao, A.; Satoh, T.; Kakuchi, T.; Chen, W. -C. Synthesis of Oligosaccharide-Based Block Copolymers with Pendent *π*-Conjugated Oligofluorene Moieties and Their Electrical Device Applications. *Macromolecules* **2015**, *48*, 3907–3917. DOI: 10.1021/acs.macromol.5b00651

(24) Breitenbach, B. B.; Schmid, I.; Wich, P. R. Amphiphilic Polysaccharide Block Copolymers for pH-Responsive Micellar Nanoparticles. *Biomacromolecules* **2017**, *18*, 2839–2848. DOI: 10.1021/acs.biomac.7b00771

(25) Zhang, N.; Wardwell, P. R.; Bader, R. A. Polysaccharide-Based Micelles for Drug Delivery. *Pharmaceutics* **2013**, *5*, 329–352. DOI: 10.3390/pharmaceutics5020329

(26) Zhao, Z.; Zhang, Z.; Chen, L.; Cao, Y.; He, C.; Chen, X. Biodegradable Stereocomplex Micelles Based on Dextran-*block*-Polylactide as Efficient Drug Deliveries. *Langmuir* **2013**, *29*, 13072–13080. DOI: 10.1021/la402890k

(27) Ceresa, R. J. The Synthesis of Block and Graft Copolymers of Cellulose and Its Derivatives. *Polymer.* **1961**, *2*, 213–219. DOI: 10.1016/0032-3861(61)90024-6

(28) Yagi, S.; Kasuya, N.; Fukuda, K. Synthesis and characterization of cellulose-*b*-polystyrene. *Polym. J.* **2010**, *42*, 342–348. DOI: 10.1038/pj.2009.342

(29) Houga, C.; Meins, J. -F. Le; Borsali, R.; Taton, D.; Gnanou, Y. Synthesis of ATRP-induced dextran-*b*-polystyrene diblock copolymers and preliminary investigation of their self-assembly in water. *Chem. Commun.* **2007**, *29*, 3063–3065. DOI: 10.1039/b706248f

(30) Li, B. -G.; Zhang, L. -M. Synthesis and characterization of novel amphiphilic block copolymers based on maltoheptaose and poly(ε-caprolactone). *Carbohydr. Polym.* **2008**, *74*, 390–395. DOI: 10.1016/j.carbpol.2008.03.009

(31) Volokhova, A. S.; Edgar, K. J.; Matson, J. B. Polysaccharide-containing block copolymers: synthesis and applications. *Mater. Chem. Front.* **2020**, *4*, 99–112. DOI: 10.1039/c9qm00481e

(32) Golas, P. L.; Matyjaszewski, K. Marrying Click Chemistry with Polymerization: Expanding the Scope of Polymeric Materials. *Chem. Soc. Rev.* **2010**, *39*, 1338–1354. DOI: 10.1039/b901978m

(33) Rostovtsev, V. V.; Green, L. G.; Fokin, V. V.; Sharpless, K. B. A Stepwise Huisgen Cycloaddition Process: Copper(I)-Catalyzed Regioselective "Ligation" of Azides and

Terminal Alkynes. *Angew. Chemie. Int. Ed.* **2002**, *41*, 2596–2599. DOI: 10.1002/1521-3773(20020715)41:14<2596::AID-ANIE2596>3.0.CO;2-4

(34) Worrell, B. T.; Malik, J. A.; Fokin, V. V. Direct Evidence of a Dinuclear Copper Intermediate in Cu(I)-Catalyzed Azide-Alkyne Cycloadditions. *Science* **2013**, *340*, 457–461. DOI: 10.1126/science.1229506

(35) Puls, J.; Wilson, S. A.; Hölter, D. Degradation of Cellulose Acetate-Based Materials: A Review. *J. Polym. Environ.* **2011**, *19*, 152–165. DOI: 10.1007/s10924-010-0258-0

(36) Edgar, K. J.; Buchanan, C. M.; Debenham, J. S.; Rundquist, P. A.; Seiler, B. D.; Shelton, M. C.; Tindall, D. Advances in cellulose ester performance and applicaton. *Prog. Polym. Sci.* **2001**, *26*, 1605–1688. DOI: 10.1016/S0079-6700(01)00027-2

(37) Arrington, K. J.; Haag, J. V.; French, E. V.; Murayama, M.; Edgar, K. J.; Matson, J. B. Toughening Cellulose: Compatibilizing Polybutadiene and Cellulose Triacetate Blends. *ACS Macro Lett.* **2019**, *8*, 447–453. DOI: 10.1021/acsmacrolett.9b00136

(38) Kamitakahara, H.; Enomoto, Y.; Hasegawa, C.; Nakatsubo, F. Synthesis of diblock copolymers with cellulose derivatives. 2. Characterization and thermal properties of cellulose triacetate-clock-oligoamide-15. *Cellulose* **2005**, *12*, 527–541. DOI: 10.1007/s10570-005-7135-3

(39) Chen, J.; Kamitakahara, H.; Edgar, K. J. Synthesis of polysaccharide-based block copolymers via olefin cross-metathesis. *Carbohydr. Polym.* **2020**, *229*, 115530. DOI: 10.1016/j.carbpol.2019.115530

(40) Hiraishi, M.; Igarashi, K.; Kimura, S.; Wada, M.; Kitaoka, M.; Samejima, M. Synthesis of highly ordered cellulose II in vitro using cellodextrin phosphorylase. *Carbohydr. Res.* **2009**, *344*, 2468–2473. DOI: 10.1016/j.carres.2009.10.002

(41) Nohara, T.; Sawada, T.; Tanaka, H.; Serizawa, T. Enzymatic Synthesis of Oligo(ethylene Glycol)-Bearing Cellulose Oligomers for in Situ Formation of Hydrogels with Crystalline Nanoribbon Network Structures. *Langmuir* **2016**, *32*, 12520–12526. DOI: 10.1021/acs.langmuir.6b01635

(42) Pylkkänen, R.; Mohammadi, P.; Arola, S.; De Ruijter, J. C.; Sunagawa, N.; Igarashi, K.; Penttilä, M. *In Vitro* Synthesis and Self-Assembly of Cellulose II Nanofibrils Catalyzed by the Reverse Reaction of *Clostridium Thermocellum* Cellodextrin Phosphorylase. *Biomacromolecules* **2020**, *21*, 4355–4364. DOI: 10.1021/acs.biomac.0c01162

(43) Serizawa, T.; Kato, M.; Okura, H.; Sawada, T.; Wada, M. Hydrolytic activities of artificial nanocellulose synthesized via phosphorylase-catalyzed enzymatic reactions. *Polym. J.* **2016**, *48*, 539–544. DOI: 10.1038/pj.2015.125

(44) Yataka, Y.; Sawada, T.; Serizawa, T. Enzymatic synthesis and post-functionalization of two-dimensional crystalline cellulose oligomers with surface-reactive groups. *Chem. Commun.* **2015**, *51*, 12525–12528. DOI: 10.1039/c5cc04378f

(45) Krishnareddy, M.; Kim, Y. -K.; Kitaoka, M.; Mori, Y.; Hayashi, K. Cellodextrin Phosphorylase from *Clostridium Thermocellum* YM4 Strain Expressed in *Escherichia Coli*. *J. Appl. Glycosci.* **2002**, *49*, 1–8. DOI: 10.5458/jag.49.1

(46) Kamitakahara, H.; Enomoto, Y.; Hasegawa, C.; Nakatsubo, F. Synthesis of diblock copolymers with cellulose derivatives. 2 . Characterization and thermal properties of cellulose triacetate-block-oligoamide-15. *Cellulose* **2005**, *12*, 527–541. DOI: 10.1007/s10570-005-7135-3

(47) Sakai-otsuka, Y.; Zaioncz, S.; Otsuka, I.; Halila, S.; Rannou, P.; Borsali, R. Self-Assembly of Carbohydrate-*block*-Poly(3-hexylthiophene) Diblock Copolymers into Sub-10 nm Scale Lamellar Structures. *Macromoleculse* **2017**, *50*, 3365–3376. DOI: 10.1021/acs.macromol.7b00118

(48) Roche, E.; Chanzy, H.; Boudeulle, M.; Marchessault, R. H.; Sundararajan, P. Three-Dimensional Crystalline Structure of Cellulose Triacetate II. *Macromolecules* **1978**, *11*, 86–94. DOI: 10.1021/ma60061a016

(49) Takahashi, Y.; Nishikawa, S. Crystal Structure of Amylose Triacetate I. *Macromolecules* **2003**, *36*, 8656–8661. DOI: 10.1021/ma030288n

(50) Martello, M. T.; Burns, A.; Hillmyer, M. Bulk Ring-Opening Transesterification Polymerization of the Renewable *δ*-Decalactone Using an Organocatalyst. *ACS Macro Lett.* **2012**, *1*, 131–135. DOI: 10.1021/mz200006s

(51) Hamley, I. W.; Castelletto, V. Small-angle scattering of block copolymers in the melt, solution and crystal states. *Prog. polym. Sci.* **2004**, *29*, 909–948. DOI: 10.1016/j.progpolymsci.2004.06.001

(52) Jiang, X.; Kitamura, S.; Sato, T.; Terao, K. Chain Dimensions and Stiffness of Cellulosic and Amylosic Chains in an Ionic Liquid: Cellulose, Amylose, and an Amylose Carbamate in BmimCl. *Macromolecules* **2017**, *50*, 3979–3984. DOI: 10.1021/acs.macromol.7b00389

(53) Seger, B.; Aberle, T.; Burchard, W. Solution Behaviour of Cellulose and Amylose in Iron-Sodiumtartrate (FeTNa). *Carbohydr. Polym.* **1996**, *31*, 105–112. DOI: 10.1016/S0144-8617(96)00080-X

(54) Watanabe, S.; Takai, M.; Hayashi, J. An X-Ray Study of Cellulose Triacetate. *J. Polym. Sci. Part C* **1968**, *23*, 825–835.

(55) Braun, J. L.; Kadla, J. F. CTA III: A Third Polymorph of Cellulose Triacetate. *J. Carbohydr. Chem.* **2013**, *32*, 120–138. DOI: 10.1080/07328303.2012.752493

(56) Liang, G. D.; Xu, J. -T.; Fan, Z. -Q.; Mai, S. -M.; Ryan, A. J. Thin Film Morphology of Symmetric Semicrystalline Oxyethylene/Oxybutylene Diblock Copolymers on Silicon. *Macromolecules* **2006**, *39*, 5471–5478. DOI: 10.1021/ma060405p

(57) Wang, W.; Schlegel, R.; White, B. T.; Williams, K.; Voyloy, D.; Steren, C. A.; Goodwin, A.; Coughlin, E. B.; Gido, S.; Beiner, M.; Hong, K.; Kang, N. -G.; Mays, J. High Temperature Thermoplastic Elastomers Synthesized by Living Anionic Polymerization in Hydrocarbon Solvent at Room Temperature. *Macromolecules* **2016**, *49*, 2646–2655. DOI: 10.1021/acs.macromol.5b02642

(58) Sikorski, P.; Wada, M.; Heux, L.; Shintani, H.; Stokke, B. T. Crystal Structure of Cellulose Triacetate I. *Macromolecules* **2004**, *37*, 4547–4553. DOI: 10.1021/ma0498520

(59) Zugenmaier, P.; Steinmeier, H. Conformation of some amylose triesters: The influence of side groups. *Polymer* **1986**, *27*, 1601–1608. DOI: 10.1016/0032-3861(86)90111-4

For Table of Contents Use only

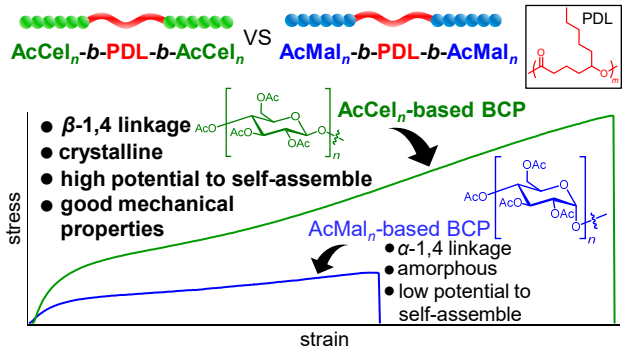

SYNOPSIS: Environmentally friendly cellulose-based block copolymers were self-assembled and exhibited higher mechanical strength than commercially available thermoplastic elastomers.